PCCP

Accepted Manuscript

ROYAL SOCIETY OF CHEMISTRY

www.rsc.org/pccp

Chemical Science

RSCPublishing

ARTICLE

Charge Transfer and Recombination at the Metal Oxide/$CH_3NH_3PbClI_2$/*spiro*-OMeTAD Interfaces: Uncovering the Detailed Mechanism behind High Efficiency Solar Cells

Cite this: DOI: 10.1039/x0xx00000x

Received 00th January 2012,
Accepted 00th January 2012

DOI: 10.1039/x0xx00000x

www.rsc.org/

Qing Shen[a,e,*], Yuhei Ogomi[b,e], Jin Chang[a], Syota Tsukamoto[b], Kenji Kukihara[b], Takuya Oshima[a], Naoya Osada[a,c], Kenji Yoshino[d,e], Kenji Katayama[c], Taro Toyoda[a,e] and Shuzi Hayase[b,e,*]

In recent years, organometal halide perovskite-based solid-state hybrid solar cells have attracted unexpected increasing interest because of their high efficiency (the record power conversion efficiency has been reported to be over 15%) and low fabrication cost. It has been accepted that the high efficiency was mainly attributed to the strong optical absorption (absorption coefficient: 15000 cm^{-1} at 550 nm) over a broader range (up to 800 nm) and the long lifetimes of photoexcited charge carriers (in the order of 10 ns – a few 100 ns) of the perovskite absorbers. However, much of the fundamental photophysical properties of perovskite relating to the high photovoltaic performance are remained to be investigated. The charge separation and recombination processes at the material interfaces are particularly important for solar cell performances. To better understand the high efficiency of perovskite solar cells, we systematically investigated the charge separation (electron and hole injection) and charge recombination dynamics of $CH_3NH_3PbClI_2$ hybrid solar cells employing TiO_2 nanostructures as the electron transfer material (ETM) and *spiro*-OMeTAD as the hole transfer material (HTM). The measurements were carried out using transient absorption (TA) techniques for a time scale from sub-picoseconds to milliseconds. We clarified the timescales of electron injection, hole injection, and recombination processes in TiO_2/$CH_3NH_3PbClI_2$/*spiro*-OMeTAD solar cells. Charge separation and collection efficiency of the perovskite-based solar cells were discussed. In addition, the effect of TiO_2 size on the charge separation and recombination dynamics was also investigated. It was found that all TiO_2-based perovskite solar cells possessed similar charge separation processes, but quite different recombination dynamics. Our results indicate that charge recombination was crucial to the performance of the perovskite solar cells, which could be effectively suppressed through optimising nanostructured TiO_2 films and surface passivation, thus pushing these cells to even higher efficiency.

Introduction

Over the past two years, a new type of organic-inorganic hybrid solid-state solar cell based on organometal trihalide perovskite has attracted unexpected increasing attention.[1-9] The organometal trihalide perovskites in the form of $CH_3NH_3PbCl_xI_{3-x}$ ($0 \le x \le 1$) can be simply crystallized from solution at low temperature (≤100 °C), which enables them as promising light absorbing materials in various solar cells. In 2009, Miyasaka and co-workers reported the first lead halide perovskite sensitized solar cells with an energy conversion efficiency of about 3.8%. However, these cells were unstable due to the iodide/triiodide redox liquid electrolyte.[10] Therefore, Nam-Gyu Park and co-workers improved the cells by further optimization of the titania surface and perovskite processing in 2011, which pushed the energy conversion efficiency up to

6.54%.[11] Since then, the perovskite-based solid-state solar cells have been reported with an unexpected rapid improvement in the energy conversion efficiency from 8% to 15.4%, as reported by the pioneering researchers of Snaith, Miyasaka, Nam-Gyu Park, and Gratzel groups.[1-9] Up to date, two kinds of architectures for the heterojunction perovskite hybrid solar cells have been proposed. One is the same as the solid-state dye-sensitized solar cells (ssDSSCs), which employs mesoporous metal oxides as an electron transport material (ETM), perovskite as the light absorber, and *spiro*-OMeTAD as the hole transport material (HTM).[1, 2, 5] Another architecture is a much simpler planar heterojunction (i.e., a p-i-n) solar cell[12] without the use of mesoporous metal oxide layer. Both of them have shown high energy conversion efficiency of over 15%, which confirms the superiority of perovskite over other light absorbing materials. Therefore, the perovskite-based solid-state solar cells are expected to be a new type of low-cost high efficiency next generation solar cells. However, the detailed mechanisms, especially the charge transfer and recombination at the interfaces within these high performance solar cells are unclear. Nam-Gyu Park has predicted that the heterojunction perovskite solar cell could achieve an efficiency as high as 20% in the near future.[4] Snaith predicts that the energy conversion efficiency of the perovskite-based solid-state solar cells is likely to be pushed toward that of CIGS (20%) and then toward and beyond that of crystalline silicon (25%) by using three key strategies: optimizing the solar cell architecture; employing a narrower band-gap perovskite; and adopting a multijunction approach.[13] To achieve these exciting goals, it is critical to gain the basic understanding of the photophysical properties, including photoexcited charge carrier dynamics, charge separation, charge recombination and charge transport in the perovskite-based hybrid solid-state solar cells. Very recently, Stranks[14] and Xing[15] reported that the effective diffusion lengths of charge carriers were relatively large in $CH_3NH_3PbI_3$ and $CH_3NH_3PbClI_2$, with the value about 100 nm and 1 μm, respectively. The relatively large charge carrier diffusion lengths arise from the higher mobility and larger charge carrier lifetimes in these materials. Therefore, light-generated electrons and holes can move ultra-long distances in the perovskite, resulting in the generation of photocurrent, instead of losing their energy as heat within solar cells. On the other hand, the charge separation and recombination dynamics at the ETM/perovskite/HTM interfaces are also significant for understanding the mechanism behind photovoltaic performances, and shedding light on the ways to even higher efficiency of perovskite solar cells.

Herein, to investigate the mechanism of high efficiency perovskite-based hybrid solid-state solar cells and therefore find similar materials for the next generation solar cells, we fabricated $CH_3NH_3PbClI_2$ perovskite hybrid solid-state solar cells employing mesoporous metal oxide films as the ETM and *spiro*-OMeTAD as the HTM. The charge separation and recombination dynamics in these cells were systematically investigated by using femtosecond and nanosecond TA techniques for a time scale of sub-picoseconds to milliseconds. To verify whether there is charge transfer from perovskite to TiO_2 and from perovskite to *spiro*-OMeTAD, and investigate the corresponding charge transfer kinetics at these interfaces, $CH_3NH_3PbClI_2$ was deposited on two types of mesoporous metal oxide films with different band gap energies (E_g). One is the commonly used titania (TiO_2) with the band gap of 3.2 eV. Another mesoporous film is yttrium oxide (Y_2O_3), which possesses a relatively wide band gap of 6.0 eV. The effect of hole transport material (*spiro*-OMeTAD) was also investigated by fabricating two types of samples, i.e. with or without *spiro*-OMeTAD. It was observed that electrons were effectively injected from perovskite into the conduction band of TiO_2, but this process was not observed in the case of Y_2O_3. This is because the conduction band edge of $CH_3NH_3PbClI_2$ is higher than that of TiO_2 but much lower than that of Y_2O_3 (Fig. 1). By choosing the probe light wavelength from the visible region to the NIR region in TA measurements, the relaxation dynamics of electrons in $CH_3NH_3PbClI_2$ and/or those injected into TiO_2, and the relaxation dynamics of holes in *spiro*-OMeTAD were detected. Photoexcited charge carrier lifetimes in $CH_3NH_3PbClI_2$, time scales of charge separation and charge recombination at the $TiO_2/CH_3NH_3PbClI_2$/*spiro*-OMeTAD interfaces were clarified. Finally, to search for the possible factors influencing the efficiency

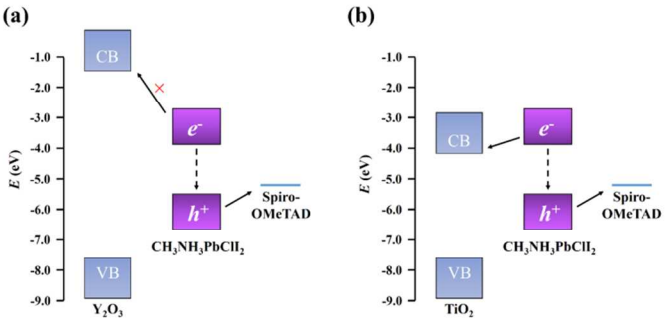

Fig. 1 Schematic of relative energy levels in (a) $Y_2O_3/CH_3NH_3PbClI_2$/*spiro*-OMeTAD and (b) $TiO_2/CH_3NH_3PbClI_2$/*spiro*-OMeTAD.

of perovskite-based solar cells, we compared the photoexcited charge carrier dynamics between two kinds of $TiO_2/CH_3NH_3PbClI_2$/*spiro*-OMeTAD solar cells employing TiO_2 nanocrystals of different sizes (18 nm TiO_2 for cell A, 30 nm TiO_2 for cell B). It was observed cell B showed a much higher energy conversion efficiency (~ 9%) compared to that of cell A (~ 6%). The difference in the efficiency was suggested to be due to the great difference in the incident photon to current conversion efficiency (IPCE) and thus the resultant short circuit current density (J_{sc}). Charge separation and charge collection efficiencies were quantitatively discussed for these solar cells. It was revealed that the differences in IPCE and J_{sc} were mainly attributed to the greatly different charge recombination time, which was about one order slower in cell B compared to that in cell A.

Experimental

Sample preparation. The samples of perovskite hybrid solar cells were fabricated by the following processes and materials. F-doped SnO_2 layered glass (FTO glass, Nippon Sheet Glass Co. Ltd) was patterned by using Zn powder and 6N HCl aqueous solution. On this patterned FTO glass, titanium diisopropoxide bis(acetylacetonate) solution in ethanol was sprayed at 300 °C to prepare compact TiO_2 layers. Porous TiO_2 layer was fabricated by spin-coating a TiO_2 paste of different nanoparticle sizes (18 nm: PST-18NR or 30 nm: PST-30NRD, JGC Catalysts and Chemicals Ltd.) in ethanol (TiO_2 paste : ethanol = 1:2.5 weight ratio for PST-18NR or TiO_2 paste: ethanol = 2:7 weight ratio for PST-30NRD), followed by heating the substrate at 550 °C for 30 min. For some TA measurements, glasses, instead of FTO were used as the substrate and a porous Y_2O_3 was fabricated on the glass substrates. Then, CH_3NH_3I and $PbCl_2$ were mixed with a 3:1 molar ratio to prepare a 40 % solution of perovskite in N,N-dimethylformamide and the mixture was spin-coated on the TiO_2 and Y_2O_3 porous substrates. The substrates were heated at 100 °C for 45 minutes, followed by spin-coating a mixture of 55 mM of tert-butylpyridine, 9 mM of lithium bis(trifluoromethylsyfonyl)imide salt, and 68 mM of *spiro*-OMeTAD. Finally, Ag and Au electrodes

were fabricated by a vacuum deposition method for photovoltaic measurements. Photovoltaic performance was evaluated by using AM1.5G 100mW/cm^2 irradiance solar simulator (CEP-2000, Bunkoukeiki Inc) with a 0.4 x 0.4 cm mask.

Transient absorption measurements. We have used two kinds of TA setups to characterize the charge separation (electron injection and hole injection) (a fs TA technique: fs-TA)[16, 17] and charge recombination dynamics (a ns TA technique: ns-TA)[18-21] in the samples. In the fs-TA setup for characterization of charge separation,[16, 17] the laser source was a titanium/sapphire laser (CPA-2010, Clark-MXR Inc.) with a wavelength of 775 nm, a repetition rate of 1 kHz, and a pulse width of 150 fs. The light was separated into two parts. One part was used as a probe pulse. The other part was used to pump an optical parametric amplifier (OPA) (a TOAPS from Quantronix) to generate light pulses with a wavelength tunable from 290 nm to 3 μm. It was used as a pump light to excite the sample. In this study, a pump light wavelength of 470 nm and a probe beam wavelength of 775 nm were used. According to the experimental results reported by Deschler and co-workers very recently,[22] the TA response of ground state bleaching (GSB) for $CH_3NH_3PbClI_2$ on glass peaked at 1.65 eV that was spectrally unchanged out to times beyond 200 ns. So the probe light wavelength of 775nm (i.e., the photon energy of 1. 64 eV) used in this study is appropriate to monitor the GSB of $CH_3NH_3PbClI_2$ on Y_2O_3 and TiO_2 substrates with or without *spiro*-OMeTAD, and thus electron transfer and hole transfer processes at each interfaces can be investigated systematically.

In the ns-TA setup for characterization of charge recombination,[18-21] the pump light source was an OPO (Surelite II – 10FP) output excited by a Nd:YAG nanosecond pulse laser (Panther, Continuum, Electro-Optics Inc.). The pulse width was 5 ns, and the repetition rate was 0.5 Hz. We used a pulse light with a wavelength of 470 nm as a pump light to excite the sample. The probe light was a fiber coupled CW semiconductor. Three kinds of probe wavelengths of 785 nm, 658 nm and 1310 nm were used. The probe beam of 785 nm was used to measure the TA responses of GSB for $CH_3NH_3PbClI_2$ on Y_2O_3, i.e. the recombination of electron and holes in $CH_3NH_3PbClI_2$.[22] The probe beam of 658 nm was used to measure the trapped electrons in TiO_2[23] according to the reports of Yoshihara and co-workers, which was used to investigate charge recombination between the electrons in TiO_2 and holes in the perovskite. The probe beam of 1310 nm was used to monitor the holes in *spiro*-OMeTAD[24] and thus measure the charge recombination between holes in *spiro*-OMeTAD and the electrons in TiO_2 and/or in perovskite. For all measurements, the pump and probe lights were irradiated from the glass and the TA measurements were carried out in N_2 atmosphere.

Results and Discussion

Fig. 2 shows the room temperature optical absorption spectrum of $CH_3NH_3PbClI_2$ film on Y_2O_3 porous substrates. Similar spectra were also observed for those deposited on TiO_2 porous substrates. As shown in Fig. 2, no sharp peaks related to exciton absorption were observed in the optical absorption spectrum at room temperature. This means that photoexcited electron-hole pairs exist as free charge carriers or very weak bound excitons rather than strong binding excitons. This can be understood by the fact that the exciton binding energy is relatively small in the three dimensional perovskite (e.g., 37 meV – 50 meV was reported for $CH_3NH_3PbI_3$), which is comparable to the thermal energy at room temperature[25]

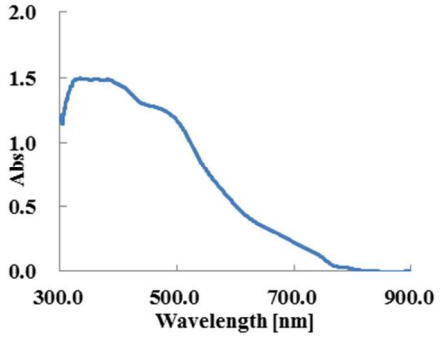

Fig. 2 Optical absorption spectrum of $CH_3NH_3PbClI_2$ at room temperature.

To systematically investigate the charge separation and recombination dynamics in $CH_3NH_3PbClI_2$-based solar cells, TA measurements were conducted for $CH_3NH_3PbClI_2$ on either Y_2O_3 or TiO_2 films, with and without *spiro*-OMeTAD. In the case of $CH_3NH_3PbClI_2$ deposited on Y_2O_3, the lifetime of photoexcited charge carriers in $CH_3NH_3PbClI_2$ and charge separation dynamics at the $CH_3NH_3PbClI_2$/*spiro*-OMeTAD interface were investigated by the fs-TA measurements. The pump light wavelength was 470 nm to only excite $CH_3NH_3PbClI_2$, and the probe light wavelength was 775 nm which was just the optical absorption edge as shown in Fig. 2.

Fig. 3(a) shows the normalized TA responses of $CH_3NH_3PbClI_2/Y_2O_3$ for a time scale up to 3 ns for different pump light intensities, i.e. 0.9 and 1.8 μJ/cm^2. A bleaching signal with a very slow decay was observed for both intensities. Since there is no electron injection from the perovskite to Y_2O_3 owing to the large band gap of Y_2O_3 (Fig. 1), the slow decay could be attributed to the slow recombination process of photoexcited charge carriers in $CH_3NH_3PbClI_2$. We confirmed that the peak intensity was proportional to the pump light intensity, but the decay time was independent of the pump light intensity as shown in Fig. 3(a). We found that there were two processes in the TA decay process and the TA signal could be well-fitted to the following biexponential function:

$$Y = A_1 e^{-t/t_1} + A_2 e^{-t/t_2} \qquad (1)$$

where t_1 and t_2 are the time constants, A_1 and A_2 are the contributions from the corresponding components. It was calculated that the time constants t_1 and t_2 of the two charge recombination processes are 34 ps ($A_1/(A_1+A_2)$: 9%) and much larger than 10 ns ($A_2/(A_1+A_2)$: 91%), respectively. The faster decay process (34 ps) could be considered to be nonradiative recombination of electrons and holes through defects or trap states in $CH_3NH_3PbClI_2$ or at $CH_3NH_3PbClI_2/Y_2O_3$ interfaces. This is consistent with the observations reported by Deschler and co-workers very recently that the photoluminescence quantum efficiency (PLQE) was lower at lower pump intensity (<25 mW/cm^2) but increased rapidly above 50% for higher pump intensity (by 100 mW/cm^2) and reached a maximum value of 70% for $CH_3NH_3PbClI_2$ on glass. Their results and our result indicated the possibility of nonradiative recombination due to effects at lower pump light excitation. However, as shown in Fig. 3, the relative contribution of the faster decay is as small as less than 10%, which suggested that the defect or trap state density in $CH_3NH_3PbClI_2$ or at the interfaces is very small, which was consistent with the previous results obtained by a thermally stimulated current measurement.[26] The slower decay process (>> 3 ns) could be attributed to the recombination of free

electrons and holes in $CH_3NH_3PbClI_2$. This result suggested that the lifetime of photoexcited charge carriers was quite long, which was confirmed to be as long as μs by the following ns-TA measurement results.

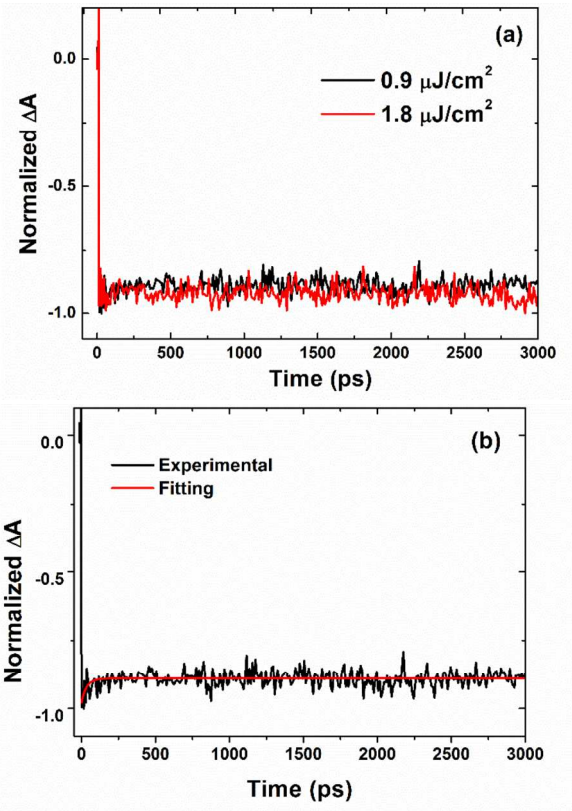

Fig. 3 (a) Dependence of normalized TA responses of $CH_3NH_3PbClI_2/Y_2O_3$ on pump light intensity and (b) experimental and theoretical fitting results with a biexponential function (eq. (1)).

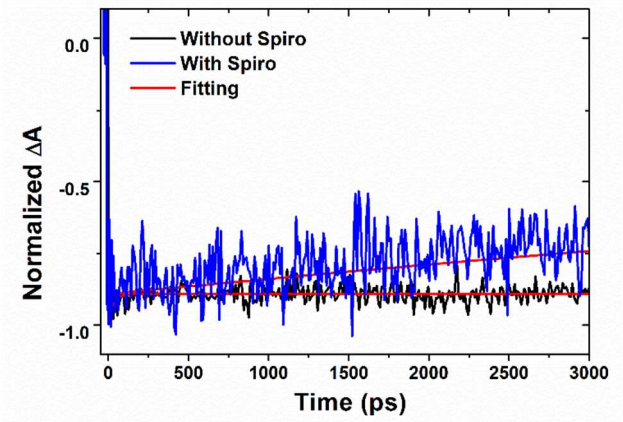

Fig. 4 Normalized TA responses of $CH_3NH_3PbClI_2/Y_2O_3$ with and without *spiro*-OMeTAD as a HTM. The red solid lines represent the fitting results with eq. (1).

Figure 4 shows the normalized TA responses of $CH_3NH_3PbClI_2/Y_2O_3$ samples with and without *spiro*-OMeTAD as the HTM. By fitting the TA response of $CH_3NH_3PbClI_2/Y_2O_3$ with *spiro*-OMeTAD to eq. (1), we found that only one exponential decay with a time constant of 16±2 ns appeared. Comparing with the long lifetime (as long as microseconds as shown below) of the TA decay in $Y_2O_3/CH_3NH_3PbClI_2$, the fast decay process in the $Y_2O_3/CH_3NH_3PbClI_2$/*spiro*-OMeTAD could be considered to originate from the photoexcited hole injection from $CH_3NH_3PbClI_2$ to *spiro*-OMeTAD. This result indicated that charge separation occurred at the interfaces between $CH_3NH_3PbClI_2$ and *spiro*-OMeTAD. In fact, we also tried to measure the TA signal of holes in *spiro*-OMeTAD using the pump wavelength of 470 nm and probe beam wavelength of 1310 nm using the fs-TA, since the holes in *spiro*-OMeTAD could show a TA signal in the NIR region.[24] However, we couldn't observe any TA signal for the 1310 nm probe for the time scale up to 3 ns. This is possibly due to the longer hole transfer time of 16 ns. On the other hand, as shown below (Fig. 6), the TA signal of holes in *spiro*-OMeTAD with 1310 nm probing were observed very clearly in the time scale of μs. This result also supported the longer hole injection time of 16 ns in this case.

Following the fs-TA measurements, ns-TA setup was applied to measure the TA responses of $CH_3NH_3PbClI_2/Y_2O_3$ (with and without *spiro*-OMeTAD) samples to further study the charge carrier lifetimes and charge recombination between electrons in $CH_3NH_3PbClI_2$ and holes in *spiro*-OMeTAD. Figure 5 shows the TA responses of $CH_3NH_3PbClI_2/Y_2O_3$ without *spiro*-OMeTAD for a time scale of 200 μs measured with a pump light wavelength of 470 nm and a probe light wavelength of 785 nm. Similar to the fs TA results shown in Fig. 3, a large bleaching signal was observed and recovered to zero at around 100 μs. This is considered to be the recombination of electrons and holes in $CH_3NH_3PbClI_2$, because there is no electron injection to Y_2O_3 just as mentioned above. By fitting the TA decay with eq. (1), we found that two decay processes existed with lifetimes of 3.7±0.1 μs (70%) and 60±1 μs (30%), respectively. Combing the fs-TA and ns-TA results for $CH_3NH_3PbClI_2/Y_2O_3$, the lifetime of photoexcited charge carriers in $CH_3NH_3PbClI_2$ can be mainly considered to be as long as μs.

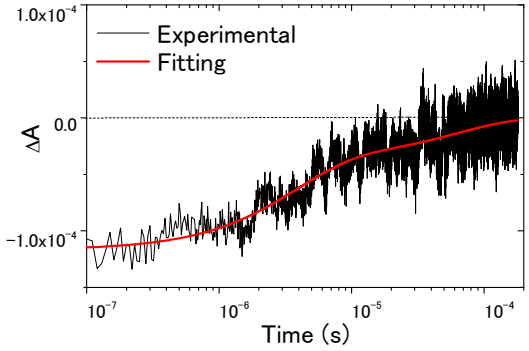

Fig. 5 TA responses of $CH_3NH_3PbClI_2/Y_2O_3$ without *spiro*-OMeTAD for a time scale of 200 μs measured with a pump light wavelength of 470 nm and a probe light wavelength of 785 nm. The red solid lines represent the fitting results with eq. (1).

Figure 6 shows TA response of $CH_3NH_3PbClI_2/Y_2O_3$ with *spiro*-OMeTAD as the HTM measured at a probe wavelength of 1310 nm. This result indicates that charge separation truly occurred at the $CH_3NH_3PbClI_2$/*spiro*-OMeTAD interfaces, which is well consistent with the fs-TA result as shown in Fig. 4. The decrease of the TA signal of $CH_3NH_3PbClI_2/Y_2O_3$ with *spiro*-OMeTAD originated from the recombination between the electrons in $CH_3NH_3PbClI_2$ and the holes in *spiro*-OMeTAD, which could be fitted very well with eq. (1) and only one exponential decay was observed. The time constant

of the decay was determined to be 0.37±0.07 μs, which corresponded to the recombination time.

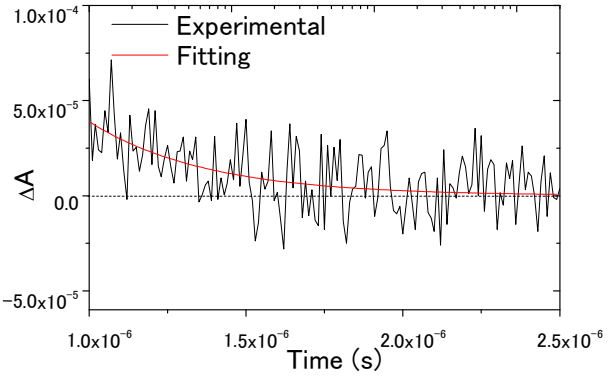

Fig. 6 TA responses of $CH_3NH_3PbClI_2/Y_2O_3$ with *spiro*-OMeTAD measured with a pump light wavelength of 470 nm and a probe light wavelength of 1310 nm. The red solid lines represent the fitting results with eq. (1).

Based on the above results, the photoexcited charge carrier (electrons and holes) dynamics in $CH_3NH_3PbClI_2$ deposited on Y_2O_3 substrate without and with *spiro*-OMeTAD as a HTM were clarified, which are illustrated in Figure 7.

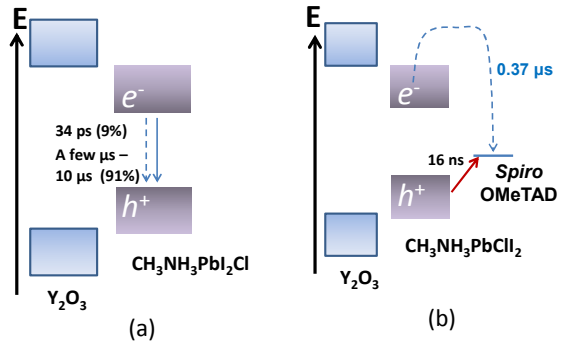

Fig. 7 Schematic illustration of photoexcited charge carrier (electrons and holes) dynamics in $CH_3NH_3PbClI_2$ deposited on Y_2O_3 substrate without (a) and with (b) *spiro*-OMeTAD as a HTM.

Subsequently, we studied the photoexcited electron injection and recombination dynamics using both the fs-TA and ns-TA measurements for $CH_3NH_3PbClI_2$ deposited on TiO_2 substrates. Figure 8(a) shows the normalized TA responses of $CH_3NH_3PbClI_2/TiO_2$ for 400 ps with the pump light intensities ranging from 0.5 μJ/cm^2 to 12.5 μJ/cm^2. Similar to $CH_3NH_3PbClI_2$ deposited on Y_2O_3, when the pump light intensity was lower, the decays in the normalized TA responses overlapped with each other very well. However, when the pump light intensity was larger than 3.75 μJ/cm^2, a faster decay process appeared in the TA response, which maybe resulted from interactions of multiple charge carriers (e.g., Auger recombination). To determine the electron injection dynamics from $CH_3NH_3PbClI_2$ to TiO_2, the TA response of $CH_3NH_3PbClI_2/TiO_2$ under a lower pump light intensity (i.e., the decay was independent of pump light intensity) was used to compare with that of $CH_3NH_3PbClI_2/Y_2O_3$. As shown in Fig. 7(b), the TA response of $CH_3NH_3PbClI_2/TiO_2$ decayed much faster than that of $CH_3NH_3PbClI_2/Y_2O_3$ and can be fitted very well to a one exponential decay function with a time constant of 1.8±0.1 ns, which is about 2 - 3 orders smaller than the photoexcited charge carrier lifetimes (~μs) as shown in Fig. 7. It is worth noting that the fast decay component with a lifetime of 34 ps that appeared in the TA response of $CH_3NH_3PbClI_2/Y_2O_3$ is not observed in that of $CH_3NH_3PbClI_2/TiO_2$. So the electron injection time t_{ET} and electron injection rate k_{ET} can be calculated to be about 1.8 ns and 5.5×10^8 s^{-1} by the following equation:

$$k_{ET} = 1/t_{ET} = 1/t_{Pero/TiO_2} - 1/t_{Pero/Y_2O_3} \quad (2)$$

where $t_{Pero/TiO2}$ and $t_{Pero/Y2O3}$ are the TA signal decay times of the perovskite on TiO_2 and Y_2O_3 substrates, respectively. Then, the electron injection efficiency η_{Einj} can be calculated to be about 100% for all electrons with lifetimes longer than 100 ns. Here we suppose that the other 9% charge carriers that recombined with a lifetime of 34 ps did not exist in the $CH_3NH_3PbClI_2$ prepared on TiO_2, because we didn't observe any faster decay component in the TA responses of $CH_3NH_3PbClI_2/TiO_2$.

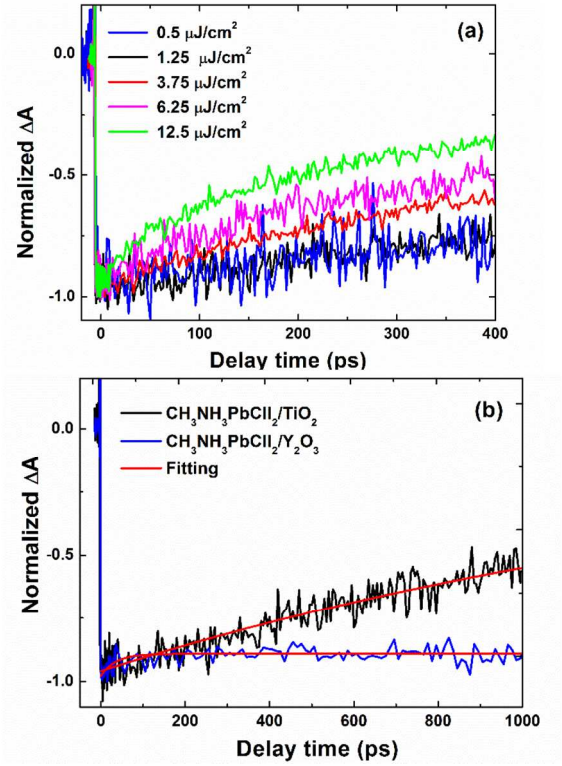

Fig. 8 (a) Dependence of normalized TA responses of $CH_3NH_3PbClI_2/TiO_2$ on pump light intensity and (b) theoretical fitting result of the TA response (pump light intensity: 1.25 μJ/cm^2) with a biexponential function (eq. (1)). For comparison, the TA response of $CH_3NH_3PbClI_2/Y_2O_3$ is also shown in (b). The pump light wavelength is 470 nm and the probe light wavelength is 775 nm.

Next, we detected the recombination dynamics in $CH_3NH_3PbClI_2/TiO_2$ without *spiro*-OMeTAD, i.e., the recombination between electrons in TiO_2 and holes in $CH_3NH_3PbClI_2$, using the ns-TA. Figure 9 shows the TA response of $CH_3NH_3PbClI_2/TiO_2$ measured with a pump light wavelength of 470 nm and a probe light wavelength of 658 nm. Yoshihara and co-workers have clearly demonstrated that TA signal in nanocrystalline TiO_2 films observed at 500 nm – 1000 nm mostly resulted from trapped electrons in TiO_2[23]. In addition, in the previous studies,[18-21] it was shown that electrons injected into TiO_2 from DSC and QDSCs could be detected by the TA signal probed at 658 nm in the timescale of microseconds. We also measured TA response of $CH_3NH_3PbClI_2/Y_2O_3$ under the same condition and observed a bleach signal as shown in Fig. S1 in the supporting information. Therefore, it is reasonable to think that the TA response in $CH_3NH_3PbClI_2/TiO_2$ observed at 658 nm corresponded to the electrons in TiO_2 injected from $CH_3NH_3PbClI_2$. As shown in Figure 9, the TA decay can be fitted very well with a one exponential function with a time constant of 0.14±0.02 μs. This result indicates that the recombination between electrons in TiO_2 and holes in perovskite occurred with a time t_{rec1} of 0.14 μs.

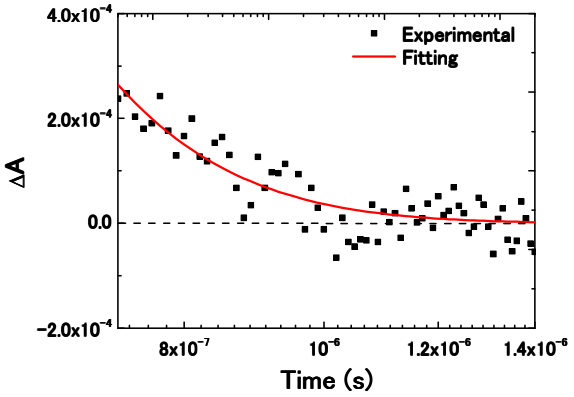

Fig. 9 TA response of $CH_3NH_3PbClI_2/TiO_2$ without a HTM measured with a pump light wavelength of 470 nm and a probe light wavelength of 658 nm. The red solid line represents the fitting result with a one exponential decay function with a time constant of 0.14 μs.

Then, we detected the recombination dynamics in $CH_3NH_3PbClI_2/TiO_2$ with *spiro*-OMeTAD, i.e., the recombination between electrons in TiO_2 and holes in *spiro*-OMeTAD using the ns-TA. Figure 10 shows TA response of $CH_3NH_3PbClI_2/TiO_2$ without (a) and with (b) *spiro*-OMeTAD measured with a pump light wavelength of 470 nm and a probe light wavelength of 1310 nm, which monitors the relaxation dynamics of holes in *spiro*-OMeTAD. For the sample without *spiro*-OMeTAD, no TA signal can be observed. However, for the sample with *spiro*-OMeTAD, an absorption signal can be observed very clearly, which can be fitted very well with a one exponential decay function with a time constant of 60 ±0.5 μs.

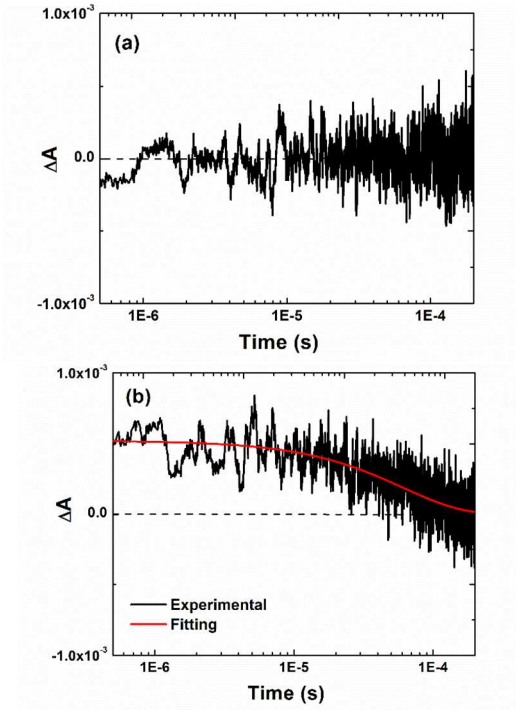

Fig. 10 TA responses of $CH_3NH_3PbClI_2/TiO_2$ without (a) and with (b) *spiro*-OMeTAD as a HTM measured with a pump light wavelength of 470 nm and a probe light wavelength of 1310 nm. The red solid line in (b) represents the fitting result with a one exponential decay function with a time constant of 60 μs.

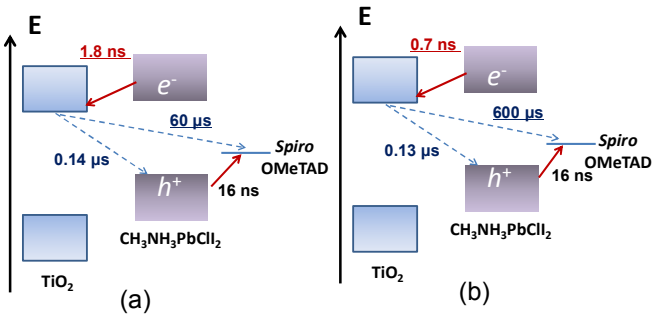

Fig. 11 Schematic illustration of photoexcited electron injection and recombination dynamics in two $TiO_2/CH_3NH_3PbClI_2$ /*spiro*-OMeTAD solar cells A (a) and B (b).

The photoexcited charge carrier relaxation and transfer dynamics of the $TiO_2/CH_3NH_3PbClI_2$/*spiro*-OMeTAD evaluated above are illustrated in Figure 11 (a). This is the typical result of the cell A with a TiO_2 nanoparticle size of 18 nm. The important thing is to understand how the carrier dynamics relate to the photovoltaic properties. We measured several cells and the energy conversion efficiency was typically 5-7%. Figure 12 (a) and (b) show typical results of the IPCE spectrum and current voltage (I-V) curve of the cell A. The short circuit current J_{sc}, open circuit voltage V_{oc}, fill factor *FF*

and energy conversion efficiency η of cell A are 11.81 mA/cm^2, 0.79 V, 0.71 and 6.59%, respectively. The IPCE value at 470 nm (the pump light wavelength used in the TA measurements) is 58%.

To investigate the effect of TiO_2 particle size on the photovoltaic performance and carrier dynamics in the TiO_2/$CH_3NH_3PbClI_2$/*spiro*-OMeTAD solar cells, we measured cell B with a TiO_2 nanoparticle size of 30 nm. The energy conversion efficiency was typically 8-10%. Figure 12 (a) and (b) also show typical results of the IPCE spectrum and current voltage (*I-V*) curve of the cell B, where J_{sc}, V_{oc}, *FF* and η are 17.60 mA/cm^2, 0.78 V, 0.69 and 9.54%, respectively. The IPCE value of cell B at 470 nm is about 85%. Comparing the photovoltaic performances of the two kinds of cells, V_{oc} and *FF* are very close to each other, but the J_{sc} values of cell B are significantly larger than those of cell A. This is due to the great difference in the IPCE spectra. To study the correlation between the photoexcited charge carrier dynamics and the photovoltaic properties, especially the IPCE, we characterized the charge separation and recombination dynamics of cell B with the same methods as mentioned for cell A. The typical result is shown in Fig. 11(b) (for the detailed TA data, please see the supporting information Figs. S2-S4). Comparing the charge carrier dynamics of the two cells, we find that the recombination time of electrons in TiO_2 and holes in the perovskite was almost the same (i.e., 0.13-0.14 μs), and the electron injection time became a little faster (0.7 ns) in the case of cell B (Fig. S2). However, the recombination time of electrons in TiO_2 and holes in *spiro*-OMeTAD in cell B became as long as 600 μs, which is ten times larger than that in cell A (60 μs). It would be very interesting and important to see how these changed separation and recombination dynamics influence the IPCE and J_{sc} of the two kinds of cells. In the following, we focus on the IPCE values at 470 nm, which are 58% and 85% for cell A and cell B, respectively.

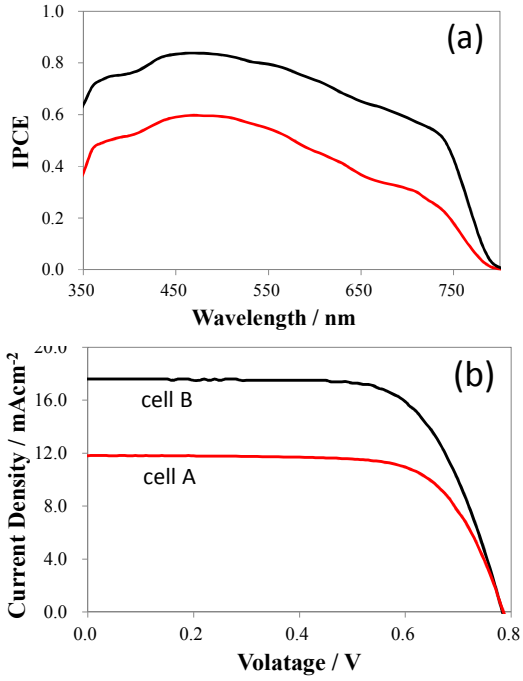

Fig. 12 Incident photon to current conversion efficiency (IPCE) spectra of the solar cells A (red) and B (black) (a) and current voltage (I-V) curves of TiO_2/$CH_3NH_3PbClI_2$/*spiro*-OMeTAD solar cells A (red) and B (black) (b).

It is known that IPCE depends on the optical absorption efficiency η_{Abs}, charge separation efficiency η_{Csep} which is the product of electron injection efficiency η_{Einj} and hole injection efficiency η_{Hinj}, and charge collection efficiency η_{Ccol} as follows:

$$IPCE = \eta_{Abs}\eta_{Csep}\eta_{Ccol} = \eta_{Abs}\eta_{Einj}\eta_{Hinj}\eta_{Ccol} \qquad (3)$$

The optical absorption of the two cells could be assumed to be almost the same here, because the perovskite is much more strongly absorbing over a broader range up to 800 nm, which can enable a complete (e.g., at 470 nm) and broader light absorption in films as thin as 500 nm.[4, 13] So we think the great difference in the IPCE as well as J_{sc} should originate from the charge separation efficiency η_{Csep} and charge collection efficiency η_{Ccol}, which are related to charge transfer and recombination rate. η_{Hinj} can be calculated using the hole injection time t_{HT} from the $CH_3NH_3PbClI_2$ to *spiro*-OMeTAD and recombination time t_{rec1} from the perovskite to TiO_2, and thus η_{Hinj} is the same for the two cells and can be estimated to be about 90% using the following equation:

$$\eta_{Hinj} = (1/t_{HT})/(1/t_{HT} + 1/t_{rec1}) \qquad (4)$$

where t_{HT} and t_{rec1} are 16 ns and 0.14 μs or 0.13μs, respectively. η_{Einj} can be considered to be close to 100% for the two cells according to the following equation (5), since the electron injection times t_{ET} from the $CH_3NH_3PbClI_2$ to TiO_2 (0.7 ns – 1.8 ns) were more than two orders smaller than the photoexcited charge carrier lifetimes $t_{lifetime}$ (as long as μs) of $CH_3NH_3PbClI_2$ and no fast recombination (observed in the case of $CH_3NH_3PbClI_2$ on Y_2O_3 substrate with a lifetime of 34 ps) was observed in $CH_3NH_3PbClI_2$/TiO_2.

$$\eta_{Einj} = (1/t_{ET})/(1/t_{ET} + 1/t_{lifetime}) \qquad (5)$$

Thus, charge separation efficiency can be considered to be about 90% for both cells. Therefore, the great difference in the IPCE of the two cells is mainly because of the difference in charge collection efficiency η_{Ccol}. Similar to solid-state DSCs, η_{Ccol} is determined by the relative diffusion time of electrons t_{Edif} through TiO_2 to the collection electrode (i.e., the FTO electrode) and the relative diffusion time of holes t_{Hdif} through *spiro*-OMeTAD to the collection electrode (i.e., the Au electrode) compared to the recombination time t_{rec2} of electrons in TiO_2 and holes in *spiro*-OMeTAD.[27] To achieve high η_{Ccol}, t_{rec2} should be much larger than t_{Edif} and t_{Hdif}, i.e., electrons and holes should arrive at the collection electrodes before their recombination with each other. In the case of cell B, the IPCE value at 470 nm is 85%, and η_{Csep} is about 90% as mentioned above. The optical absorption efficiency can be considered to be more than 90% at 470 nm considering the higher optical absorption coefficient as mentioned above, optical scattering and reflection. Then, η_{Ccol} can be considered to be close to 100% for cell B according to eq. (3). This result indicates that

the recombination time t_{rec2} of 600 μs in cell B is large enough compared to t_{Edif} and t_{Hdif} so that electrons and holes can be collected almost completely before their recombination. On the other hand, for cell A, the IPCE value at 470 nm is 58%, suggesting that η_{Ccol} is about 70% as discussed above, which is much smaller than that of cell B. This result means that the recombination time t_{rec2} of 60 μs in cell A is not large enough compared to t_{Edif} and t_{Hdif}, and thus about 30% of the charge carriers were lost due to recombination during transport of electrons in TiO_2 and holes in *spiro*-OMeTAD. These results indicate that for the perovskite-based solar cells, the key point for IPCE and J_{sc} is the charge recombination during charge carrier transport through ETM and HTM rather than charge separation or optical absorption. For a $TiO_2/CH_3NH_3PbClI_2$/*spiro*-OMeTAD solar cell device, where the thicknesses of $TiO_2/CH_3NH_3PbClI_2$ and *spiro*-OMeTAD were 500 nm and 150 nm, respectively, we find that a charge recombination time t_{rec2} in the order of a few 100 μs is long enough to achieve near complete charge collection. The reason for the great difference in t_{rec2} between cells A and B has the following possibilities. (1) The surface area of TiO_2 nanostructured layer in cell B (30 nm) is smaller than that in cell A (18 nm), thus the recombination possibility of electrons in TiO_2 and holes in *spiro*-OMeTAD was decreased greatly. (2) The TiO_2 nanostructured layer in cell B has larger pore sizes, which may result in larger crystalline perovskite growing on the TiO_2 surface. Therefore, the contact interface between TiO_2 and *spiro*-OMeTAD would decrease or the distance between them would increase. As a result, the recombination probability of electrons in TiO_2 and holes in *spiro*-OMeTAD would decrease. The details are under study now. It is beyond the scope of this paper and will be published elsewhere.

Conclusions

We systematically studied the photoexcited charge carrier dynamics of perovskite $CH_3NH_3PbClI_2$ deposited on both Y_2O_3 and TiO_2 films. We clarified the charge carrier lifetimes, charge separation and recombination dynamics in the $CH_3NH_3PbClI_2$-based solid-state hybrid solar cells, where TiO_2 was used as the ETM and *spiro*-OMeTAD was employed as the HTM. Photovoltaic properties together with charge separation and recombination dynamics of two kinds of $TiO_2/CH_3NH_3PbClI_2$/*spiro*-OMeTAD solar cells were compared, where TiO_2 nanoparticles of different sizes (Cell A: 18 nm; Cell B: 30 nm) were used in the nanostructured TiO_2 layer. Cell B showed higher IPCE, *J*sc and efficiency compared to cell A. We found that the great differences in the IPCE and J_{sc} of the two kinds of cells resulted from the great difference in charge recombination of electrons in TiO_2 and holes in *spiro*-OMeTAD. These results indicate that the key point for the IPCE and J_{sc} of the perovskite-based solar cells is charge collection efficiency, rather than charge separation efficiency. These results indicate that suppressing the recombination through appropriate interfacial engineering for the perovskite-based solid hybrid solar cells is very important for achieving high efficiency.

Acknowledgements

This research was supported by the CREST program of Japan Science and Technology Agency (JST).

Notes and references

[a] *Department of Engineering Science, The University of Electro-Communications, 1-4-1 Chofugaoka, Chofu, Tokyo 182-8585, Japan Tel:+81-424-43-5471,Fax:+81-424-43-5501, E-mail: shen@pc.uec.ac.jp*
[b] *Graduate School of Life Science and Systems Engineering, Kyushu Institute of Technology, 2-4 Hibikino, Wakamatsu, Kitakyushu 808-0196, Japan Tel: +81-936-95-6044, Fax: +81-936-95-6005, E-mail address: hayase@life.kyutech.ac.jp*
[c] *Department of Applied Chemistry, Chuo University, 1-13-27 Kasuga, Bunkyo, Tokyo 112-8551, Japan*
[d] *Department of Electrical and Electronic Engineering, Miyazaki University, 1-1 Gakuen, Kibanadai-nishi, Miyazaki 889-2192, Japan*
[e] *CREST, Japan Science and Technology Agency (JST), 4-1-8 Honcho, Kawaguchi, Saitama 332-0012, Japan*

Electronic Supplementary Information (ESI) available: [Electron injection and charge recombination dynamics of cell B]. See DOI: 10.1039/b000000x/

1. M. M. Lee, J. Teuscher, T. Miyasaka, T. N. Murakami and H. J. Snaith, *Science*, 2012, **338**, 643-647.
2. H.-S. Kim, C.-R. Lee, J.-H. Im, K.-B. Lee, T. Moehl, A. Marchioro, S.-J. Moon, R. Humphry-Baker, J.-H. Yum, J. E. Moser, M. Gratzel and N.-G. Park, *Sci. Rep.*, 2012, **2**, 591.
3. J.-H. Im, J. Chung, S.-J. Kim and N.-G. Park, *Nanoscale Research Letters*, 2012, **7**, 353.
4. N.-G. Park, *The Journal of Physical Chemistry Letters*, 2013, **4**, 2423-2429.
5. J. Burschka, N. Pellet, S.-J. Moon, R. Humphry-Baker, P. Gao, M. K. Nazeeruddin and M. Gratzel, *Nature*, 2013, **499**, 316-319.
6. D. Q. Bi, G. Boschloo, S. Schwarzmuller, L. Yang, E. M. J. Johansson and A. Hagfeldt, *Nanoscale*, 2013, **5**, 11686-11691.
7. L. Etgar, P. Gao, Z. S. Xue, Q. Peng, A. K. Chandiran, B. Liu, M. K. Nazeeruddin and M. Gratzel, *Journal of the American Chemical Society*, 2012, **134**, 17396-17399.
8. E. Edri, S. Kirmayer, D. Cahen and G. Hodes, *Journal of Physical Chemistry Letters*, 2013, **4**, 897-902.
9. G. Hodes, *Science*, 2013, **342**, 317-318.
10. A. Kojima, K. Teshima, Y. Shirai and T. Miyasaka, *Journal of the American Chemical Society*, 2009, **131**, 6050-+.
11. J.-H. Im, C.-R. Lee, J.-W. Lee, S.-W. Park and N.-G. Park, *Nanoscale*, 2011, **3**, 4088-4093.
12. M. Liu, M. B. Johnston and H. J. Snaith, *Nature*, 2013, **501**, 395-398.
13. H. J. Snaith, *The Journal of Physical Chemistry Letters*, 2013, **4**, 3623-3630.
14. S. D. Stranks, G. E. Eperon, G. Grancini, C. Menelaou, M. J. P. Alcocer, T. Leijtens, L. M. Herz, A. Petrozza and H. J. Snaith, *Science*, 2013, **342**, 341-344.
15. G. Xing, N. Mathews, S. Sun, S. S. Lim, Y. M. Lam, M. Grätzel, S. Mhaisalkar and T. C. Sum, *Science*, 2013, **342**, 344-347.
16. Q. Shen, Y. Ogomi, B.-w. Park, T. Inoue, S. S. Pandey, A. Miyamoto, S. Fujita, K. Katayama, T. Toyoda and S. Hayase, *Physical Chemistry Chemical Physics*, 2012, **14**, 4605-4613.
17. Q. Shen, Y. Ogomi, S. K. Das, S. S. Pandey, K. Yoshino, K. Katayama, H. Momose, T. Toyoda and S. Hayase, *Physical Chemistry Chemical Physics*, 2013, **15**, 14370-14376.
18. S. Kuwahara, H. Hata, S. Taya, N. Maeda, Q. Shen, T. Toyoda and K. Katayama, *Physical Chemistry Chemical Physics*, 2013, **15**, 5975-5981.

19. S. Kuwahara, S. Taya, N. Osada, Q. Shen, T. Toyoda and K. Katayama, *Physical Chemistry Chemical Physics*, 2014, **16**, 5242-5249.
20. N. Maeda, H. Hata, N. Osada, Q. Shen, T. Toyoda, S. Kuwahara and K. Katayama, *Physical Chemistry Chemical Physics*, 2013, **15**, 11006-11013.
21. N. Osada, T. Oshima, S. Kuwahara, T. Toyoda, Q. Shen and K. Katayama, *Physical Chemistry Chemical Physics*, 2014, **16**, 5774-5778.
22. F. Deschler, M. Price, S. Pathak, L. E. Klintberg, D.-D. Jarausch, R. Higler, S. Hüttner, T. Leijtens, S. D. Stranks, H. J. Snaith, M. Atatüre, R. T. Phillips and R. H. Friend, *The Journal of Physical Chemistry Letters*, 2014, **5**, 1421-1426.
23. T. Yoshihara, R. Katoh, A. Furube, Y. Tamaki, M. Murai, K. Hara, S. Murata, H. Arakawa and M. Tachiya, *The Journal of Physical Chemistry B*, 2004, **108**, 3817-3823.
24. R. Plass, S. Pelet, J. Krueger, M. Grätzel and U. Bach, *The Journal of Physical Chemistry B*, 2002, **106**, 7578-7580.
25. K. Tanaka, T. Takahashi, T. Ban, T. Kondo, K. Uchida and N. Miura, *Solid State Communications* 2003, **127**, 619-623.
26. Y. Ogomi, K. Kukihara, Q. Shen, T. Saito, K. Yoshino, S. S Pandey, T.Toyoda, H. Momose, and S. Hayase, *PVSEC-23 Proceedings, 5-O-11*, 2013, .
27. A. Hagfeldt, G. Boschloo, L. Sun, L. Kloo and H. Pettersson, *Chemical Reviews*, 2010, **110**, 6595-6663.